A Multi-DoF Exoskeleton Haptic Device for the Grasping of a Compliant Object Adapting to a User's Motion Using Jamming Transitions

Ryohei Michikawa, Takahiro Endo, *Member, IEEE*, and Fumitoshi Matsuno, *Senior Member, IEEE*

***Abstract*—In the recently growing field of virtual reality, the virtual grasping sensation remains in its infancy, and the discrepancy between real and virtual grasping has become a problem. This article develops a new haptic glove that presents the sensation of different types of grasping (e.g., power/precision/intermediate grasping) a compliant object. To this end, we develop an exoskeleton that fixes the movements of fingers to present a braking force and a flexible pad that reproduces a wide range of stiffness. By applying the "string jamming mechanism," our exoskeleton has functions that existing devices do not. In that, it constrains the motion of finger extension/flexion and adduction/abduction with only one actuator and presents the braking force to all surfaces of the finger. In addition, we propose a lightweight and compact variable-stiffness pad that reproduces an extensive stiffness range based on the layer jamming technique. We conducted experiments to evaluate the mechanical performance of the prototype integrating the exoskeleton and the variable-stiffness pad and demonstrated the usefulness of the proposed glove.**

***Index Terms*—Haptics and haptic interfaces, perception for grasping and manipulation, stiff/soft sensation, wearable robots.**

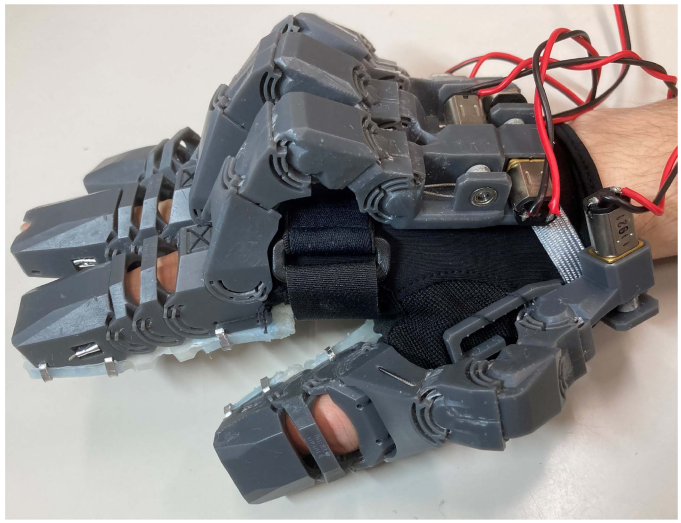

Fig. 1. Prototype device (for five fingers).

I. Introduction

THE human hand performs a variety of daily tasks, including the grasping and manipulation of objects. In particular, finger placement and human tactile perception in grasping are complex and diverse in nature [1]–[4]. According to the GRASP taxonomy [4], the most recent classification of grasping, there are 33 types of grasping. These can be broadly classified into three categories: precision grasping, in which the contact sites are only the fingertips; power grasping, in which the contact sites are over wide areas of the fingers; and intermediate grasping between precision grasping and power grasping.

In virtual reality (VR), which has rapidly advanced in recent years, it is common to use the hands to manipulate virtual objects. Additionally, in telerobotics, the usefulness of controlling manipulators in synchronization with the human arm is emphasized [5], [6]. This type of intuitive operation is essential for robot-assisted surgery. Although there has been a remarkable growth of visual and auditory information presentation in VR or telerobotics, the presentation of haptic information to the hands remains in its infancy. In particular, comprehending the sensory information of an object is essential in daily tasks such as grasping, carrying, and positioning in 3-D space [7]. In carrying out these tasks, people unconsciously use different types of grasping, such as precision grasping and power grasping, and it is necessary to develop a device that presents the appropriate sensation according to the intended grasping of the user.

There have been many attempts to develop haptic devices that present the grasp sensation. Such devices should be able to present grasping sensations and satisfy various requirements such as those of the wearability, range of motion, response speed, and reproduction of multimodal haptics. In this article, we focus on the following three requirements. 1) The device must be lightweight and easy to wear for use in VR environments. 2)

Manuscript received 30 November 2021; revised 20 April 2022; accepted 23 June 2022. Date of publication 9 August 2022; date of current version 8 February 2023. This work was supported in part by the incubation fund of Kyoto University. This paper was recommended for publication by Associate Editor R. Ozawa and Editor E. Yoshida upon evaluation of the reviewers' comments. *(Corresponding author: Ryohei Michikawa.)*

The authors are with the Department of Mechanical Engineering and Science, Graduate School of Engineering, Kyoto University, Kyoto 606-8501, Japan (e-mail: michikawa.ryohei@gmail.com; endo@me.kyoto-u.ac.jp; matsuno@me.kyoto-u.ac.jp).

This work involved human subjects or animals in its research. Approval of all ethical and experimental procedures and protocols was granted by the Ethics Committee, Graduate School of Engineering, Kyoto University (No. 202011), and performed in line with the Research on haptic devices that present and create the illusion of virtual haptic sensations.

This article has supplementary material provided by the authors and color versions of one or more figures available at https://doi.org/10.1109/TRO.2022.3192979.

Digital Object Identifier 10.1109/TRO.2022.3192979

The device must present forces for the grasping states (e.g., power/precision/intermediate grasping) that a user intends. We divide requirement 2) into three parts: 2-1) the requirement to present a force at the correct position of a hand according to the grasping state; 2-2) the requirement to present a force in the appropriate direction; 2-3) the requirement to have a sufficient range of motion for grasping movements. 3) The device must present physical characteristics of the object, such as the compliance.

There are two mechanisms of conventional haptic devices for grasping: active feedback to the finger [8]–[11] and passive feedback (i.e., a braking force) [7], [12]–[15]. Existing active feedback devices only present forces at the fingertips and do not meet requirement 2-1). In particular, these devices cannot cope with grasping that involves contact with wide areas of the fingers, such as power grasping. In addition, there is a danger of the actuators going out of control, and, thus, we did not consider active feedback in the present study. Although passive feedback devices are less dangerous because the presented force is generated by the user's grip strength, the direction of the force is limited to the bending direction of the fingers, and compliance cannot be displayed. In other words, the devices do not meet requirements 2-2) and 3).

We have applied the "string jamming mechanism" principle [16] to develop a new exoskeleton that is both flexibly deformable and fixable with various shapes. This exoskeleton satisfies requirement 1) in that it has only one actuator per finger and is lightweight. The exoskeleton also satisfies requirement 2-1) in that it covers the fingers in a glove-like manner and presents a braking force to arbitrary regions of a finger's surface. Furthermore, by fixing the shape of a finger, the braking force can be applied to any movement of the finger, thus satisfying requirement 2-2). Here, the string jamming mechanism is a bead-like multidegree of freedom (DoF) linkage mechanism proposed by Mukaide et al. [16]. This mechanism can fix the angles of all joints by generating static friction along the rotation axes through wire tension.

In addition, we have developed a flexible pad (referred to as a variable-stiffness pad) whose stiffness is continuously controllable using a material such as a powder or paper bundle that increases in stiffness through air compression [17]. As the variable-stiffness pad is compact, it does not interfere with the finger movement and allows a sufficient range of motion even though arranged on the finger's ventral. We, thus, conclude that the requirement 2-3) is satisfied. By arranging this pad on the ventral side of the finger, we can control the virtual stiffness, thus satisfying requirement 3). Here, the ventral part alone is considered sufficient because the flexible ventral tissue, rather than the side part of the finger, is primarily used in compliance perception.

In this study, we developed a device that satisfies all the requirements 1), 2), and 3) by assembling the above exoskeleton and variable-stiffness pad (Fig. 1). The prototype device is relatively light, weighing only about 60 g per finger, including the motor for driving. In addition, the device can be made entirely wearable by changing the external power source to a battery and can provide haptic feedback without interfering with the free movement of the user. Our device is potentially applicable to VR training and a variety of other VR applications, e.g., virtual reality aided design [18]–[20]. In addition, this device can be applied to robot teleoperation [5], [6] by integrating a noncontact shape and compliant measurement system [21].

II. Related Work

A. Wearability and Portability of Haptic Devices

In several studies focusing on the wearability and portability of devices, it is commonly emphasized that devices should be lightweight, easy to don and doff, and adaptable (or comfortable) for users of various size [22]–[26]. Adaptability to various sizes is a topic of our future work but can be achieved by preparing devices of multiple sizes standardized in advance.

In this article, we set a target weight of 300 g. This target is based on commercially available haptic devices such as Dexmo [27] and CyberGrasp [8]. We have succeeded in reducing the device's weight to 60 g per finger by adopting a string jamming mechanism and using vacuum jamming material, as described below. With these developments, we have achieved a device weight of 300 g for a five-finger device, which satisfies our target specification.

Furthermore, the device is assembled in a glove-like shape and can be attached by simply fastening two Velcro strips. The device can be attached to and removed from the hand within 1 min. Including the time required to attach external devices, such as a vacuum pump, to the waist, the time required to attach and remove the entire system is less than 10 min. This satisfies the requirement specified by Randazzo et al. [23]. In particular, our device is superior to devices that attach to each finger [7], [23]–[25] because the number of fingers does not affect the attachment and removal time.

B. Method of Presenting a Braking Force

To present a braking force, it is necessary to go and return between two states: a free state following the motion of the fingers and a braking state stopping the motion. The finger motion is complex and has four DoFs (three for flexion/extension and one for adduction/abduction) [28].

The simplest solution to providing a braking force is to fix the shape of the multi-DoF linkage mechanism, which is deformable following the finger movement in a free state, with actuators or brakes [29]. In general, at least the same number of actuators as the number of DoFs are required to fix the movement of the link mechanism [13], [30]. Therefore, an increase in the number of actuators means an increase in the overall weight [13]. Conventional devices cannot fix an arbitrary motion because of considerations of the overall weight [7], [12].

Another solution that is lighter than linkage mechanisms is using soft materials whose stiffness is controllable, such as layer jamming technique [14] or particle mechanical constraint [15]. However, the methods of using soft materials have the following problems. They cannot present force but only viscosity and have a long time response.

In contrast, by applying a string jamming mechanism, we have developed an exoskeleton that can deform according to the (multi-DoF) finger and brake with a single actuator. In other words, the developed exoskeleton can achieve both lightweight and multiple DoF deformable properties without using soft materials.

C. Methods of Presenting Stiffness and Softness

There are two existing methods for presenting sensations of stiffness and softness. One method provides haptic cues by controlling the contact force or contact area range [8], [11], [31], [32] and the other changes the stiffness of the area of the contact point directly [17], [33]. The former method is limited to local presentation, making it challenging to present sensations over a wide surface of the finger while maintaining a low weight and compactness. An example of the latter method, the method of Endo et al. [33], directly controls the stiffness by changing the tension of the flexible sheet using a mechanical system. Interference between mechanisms is a problem when trying to present sensations at multiple points on a finger.

In this study, we consider granular jamming and layer jamming techniques that change the stiffness of a contact area directly [17]. We refer to them as vacuum jamming techniques because the granular/layer jamming controls stiffness via a vacuum. The vacuum jamming material, where the stiffness changes, can be separated from mechanical parts, such as the vacuum pumps. The material is, therefore, lightweight and compact and can be attached to the front of the finger. We also refer to the vacuum jamming material molded to fit the shape of the finger as a variable-stiffness pad.

III. Concept of the Proposed Device

The haptic device proposed in this study is designed to present the grasping sensations of a compliant object with the user desired grasping states. It comprises an exoskeleton that presents a braking force to the fingers and a variable-stiffness pad that presents a feeling continuously from stiffness to softness.

When people grasp a real object, they preshape their fingers to adapt to the object while approaching the object [34], [35]. It is, therefore, expected that the device can reproduce virtual grasping sensations by countering the grasping motion. The braking method adopted for the proposed device differs from the conventional braking method [7], [12], [14]. The proposed device presents the braking force for any movement to whole fingers by fixing the entire shape of the exoskeleton, which covers the fingers like a glove. The user's intention of "how to grasp the object" should affect the finger movements immediately after the preshaping. The strategy of covering the fingers like a glove and fixing the exoskeleton makes it possible to present the reaction force "distribution" according to the user's finger motions. For example, the reaction force distributions are expected to be maximized at the terminal segment for precision grasping and uniformly distributed for power grasping. Our goal is to semiautomatically reproduce the reaction force distribution that the user unconsciously expects from his or her own motion and visual information through passive feedback to the whole finger. In other words, requirements 2-1) and 2-2) are satisfied. Here, the exoskeleton must present a sufficient braking force for virtual grasping. The string jamming mechanism used to fix the exoskeleton's shape can present as much braking force as necessary by increasing the wire tensile force because the holding torque is almost proportional to the tensile force. However, the tensile force required to realize a sufficient holding torque is too strong for the previously proposed string jamming mechanism. We, therefore, propose and design new string jamming units to realize an ample holding torque using a weak wire tensile force. Using the proposed jamming units, we can fabricate a lightweight mechanism that satisfies requirement 1) in that it produces the necessary wire tension with a small motor.

Furthermore, we present sensations of the stiffness and softness of a virtual object using a variable-stiffness pad assembled with the exoskeleton. The presentation of the stiffness/softness requires that the pad can change state from being sufficiently soft to being stiff. In addition, when the fingers are removed from a virtual object, the deformed pad must quickly return to the original shape through its elasticity, and its plastic deformation should thus be small. However, the existing vacuum jamming material has an insufficient stiffness range. Therefore, we propose a variable-stiffness pad with a broader range of stiffness change by combining paper and sponge layers while remaining compactness. Using this pad, our device satisfies requirements 2-3) and 3).

In the following sections, we describe the methods used to realize the proposed concept. Section IV describes how we designed several types of string jamming units to provide a sufficient braking force and how we identified the characteristics of the units to achieve the maximum holding torque by comparing the holding torques for pairs of each type of unit. Section V identifies the best vacuum jamming materials having an extensive range of stiffness and small plastic deformation. Section VI describes the prototype haptic device developed using the string jamming units (Section IV) and the vacuum jamming materials (Section V). Section VII presents the mechanical performance of the prototype measured experimentally. Section VIII summarizes the article and discusses future work.

IV. String Jamming Mechanism With a Strong Holding Torque

A. Development

As described in Section I, the link angles of string jamming mechanisms can be fixed by the friction of each rotational joint generated by the wire tension. Therefore, the holding torque is proportional to the wire tension and friction coefficient. In reducing the size and weight of the overall device, it is necessary to design string jamming units that generate a sufficient holding torque even with low wire tension.

Mukaide et al. [16] proposed bead-type and radial layer type jamming units as shown in Fig. 2. Fig. 2(a) shows bead-type units, which are the most straightforward string jamming units. The bead-type units make contact with the neighboring units through a cylindrical surface [Fig. 2(a)], and the surface not only acts as a guide of rotation but also generates friction through the

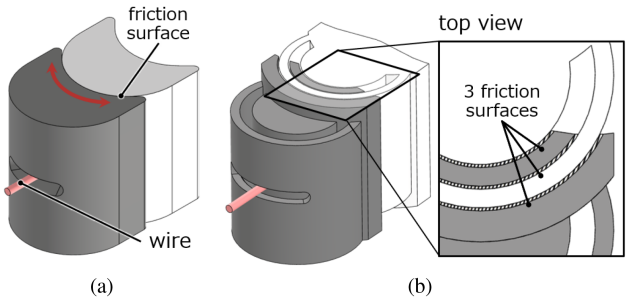

Fig. 2. Pairs of jamming units of the previous study [16]. (a) Bead-type. (b) Radial layer type without the slit element.

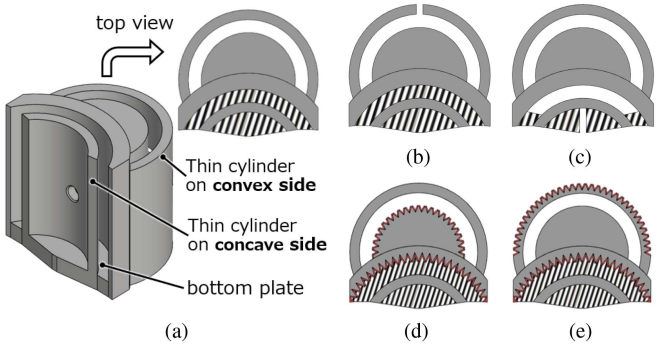

Fig. 3. Basic radial-layer unit and four elements for improvement. Grooves are highlighted in red. (a) Radial layer type unit with no additional element [same as Fig. 2(b)]. (b) Slit [16]. (c) Gap. (d) Groove. (e) Gear.

wire tension. In addition, Fig. 2(b) shows radial layer type units, which are an enhanced type of the holding torque from the bead-type. The radial layer type units have a layered structure with thin cylinders on the convex and concave sides as shown in Fig. 3(a). By appropriately combining the convex thin cylinder of one unit with the concave thin cylinder of another unit, the connection is designed to have multiple friction surfaces [Fig. 2(b) top view]. Compared with the bead-type units, where there is friction only on one surface between two units, the radial layer type units have multiple friction surfaces and generate a strong holding torque.

In addition, to improve the effect of the multilayered friction surface on the holding torque, a slit element that splits the thin convex cylinder [Fig. 3(b)] was added to the radial layer type unit in [16]. However, no study has verified the effect of the slit element in experiments, and the respective effects of the multilayered friction surface and the slit element have not been clarified. In addition, it is not known what shape characteristic maximizes the effect of the multilayered structure.

In this study, we designed and fabricated 12 types of unit combining four elements for improvement, namely the slit [Fig. 3(b)], gap [Fig. 3(c)], groove [Fig. 3(d)], and gear [Fig. 3(e)] elements, to maximize the effect of the multilayered friction surface and enhance the holding torque. The holding torques of these units were measured to identify the combination that provides the strongest braking force. Here, the gap element is an interstice of the bottom plate supporting the thin cylinder on the concave side. This element allows the concave thin cylinder

TABLE I
COMBINATIONS OF ELEMENTS FOR IMPROVEMENT

Parts no.	1	2	3	4	5	6	7	8	9	10	11	12
(b) Slit	–	✓	–	–	–	✓	✓	✓	–	–	✓	✓
(c) Gap	–	–	✓	–	–	✓	–	–	✓	✓	✓	✓
(d) Groove	–	–	–	✓	–	–	✓	–	✓	–	✓	–
(e) Gear	–	–	–	–	✓	–	–	✓	–	✓	–	✓

A ✓ mark indicates an element that is implemented in each unit.
Nos. 1 and 2, respectively, correspond to Fig. 3(a) and (b).

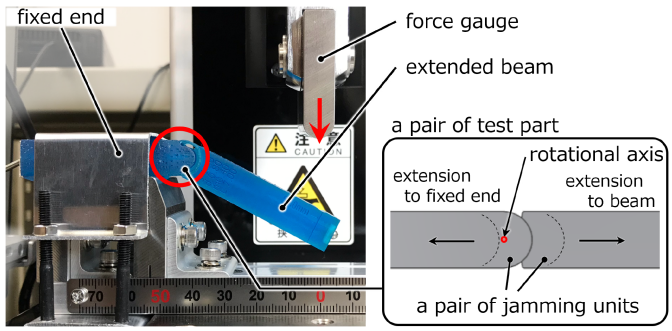

Fig. 4. Measurements of the holding torques of units.

to deflect more effectively and thus increase the contact areas of the friction surfaces. To increase the friction coefficient, we introduced grooves on the friction surfaces orthogonal to the friction direction. In particular, the groove element has grooves that do not interlock with each other, whereas the gear element has grooves that interlock with each other.

B. String Jamming Units Combining Elements for Improvement

To verify the effect of the four elements on the holding torque, we created 12 types of radial-layer unit (Nos. 1–12 in Table I). In the table, a ✓ mark indicates that the respective element was added to the basic shape (No. 1) shown in Fig. 2(b). Nos. 2–5 are units having one additional element each (Fig. 3) and Nos. 6–12 are units having multiple elements. This scheme allows the observation of the interactions of the different elements. However, the groove and gear elements were not added simultaneously because they are not independent. We carried out cantilever bending tests (Fig. 4) for the above 12 types of unit and the bead-type units (No. 0) as a nominal pair of units.

The dimensions of the experimental jamming units were an outermost radius of the cylindrical friction surface of 6 mm, a height of the cylinder of 15 mm, a thickness of each thin cylinder of 0.9 mm, and a clearance between layers of 0.1 mm. The primary purpose of the experiment was to investigate the effects of the four elements for improvement, and we, thus, used the minimum layer number (one thin cylinder on both convex and concave sides) in this experiment.

1) Measurement Method: For each pair of 13 units, we measured the holding torque according to the following procedure. Pairs of test parts corresponding to jamming units No. 0–12 in Table I are fabricated using a 3-D printer. Note that, in the 3-D printing of test parts, the stacking direction and postprocessing

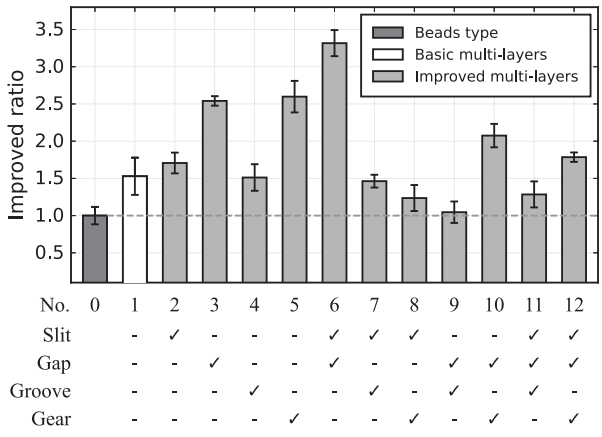

Fig. 5. Holding torque of each unit normalized by the result for the bead-type unit (No. 0). The actual torque of No. 0 is 0.080 N · m.

were standardized. One side of a part is connected to the fixed end of the measurement device and the other side is extended as a beam as shown in Fig. 4. A pair of test parts is set as a straight line and an inner wire of a part is pulled to generate the holding torque. The force gauge of the measurement device presses the point that is 5 cm from the rotational axis of the test part.

We measure the vertical force provided at the part by reading the value of the force gauge. The above procedure is regarded as one set of the experiment, and we conducted the experiment for ten sets. The holding torque is almost linear when the wire tension is in the range of 0–80 N [16]. Thus, we experimentally confirmed the property and set the wire tension in the measurement at 45 N, corresponding to roughly the middle of the linear range.

2) Results: The holding torque is calculated as

$$\tau = \frac{1}{m}\sum_{k=1}^{m} l\, F_{\max,k} \tag{1}$$

where the beam length $l = 0.05$ m, $F_{\max,k}$ is the maximum vertical force in the kth trial for each test part, and the total number of trials is $m = 10$. In addition, the results normalized by the values for the No. 0 unit are shown in Fig. 5. In the bar graph, the horizontal axis gives the "No." of each test part. An error bar represents the standard deviation of the measurements, and the dashed line indicates an improvement ratio of 1.0.

3) Discussion: First, we roughly estimate the contribution of the multilayered friction surface to the holding torque for N surfaces. When the maximum static friction force F_i is generated on the ith friction surface of radius r_i from the rotating axis, the holding torque is $r_i F_i$. If the radius of the bead-type friction surface is r_0, the holding torque is given by $\tau_0 = r_0 F_0$. When there are N friction surfaces, the holding torque τ_N for the N surfaces can be expressed as

$$\tau_N = \sum_{i=0}^{N-1} r_i F_i \tag{2}$$

where the thickness of each layer is denoted as d m and the radius of the ith friction surface is $r_i = r_0 - id$. Furthermore, we assume that the entire surface is uniformly contacted and the frictional forces acting on different friction surfaces are equal; $F_i \simeq F$. Calculation using (2) with $N = 3$, $r_0 = 6$ mm, and $d = 0.9$ mm in the experiment gives the holding torque's enhancement ratio $\tau_N/\tau_0 \simeq 2.6$. Fig. 5 shows that the enhancement ratio of No. 1 is 1.5, which is different from the calculated value of 2.6. However, the estimated values are roughly correct, and (2) can be used as a guideline for the design of a jamming unit. We consider the reason for the difference between the calculated and measured value for the No. 1 unit. One possible reason is that the rigidity of the thin cylinder is too high for the wire tension to squash the clearance, and the assumption that $F_i = F$ is thus invalid. The enhancement ratios of Nos. 2, 3, and 6 with a slit or gap element are larger than those of No. 1 because the friction surfaces made contact with each other with less tension. In particular, the units with the gap element (Nos. 3 and 6) saw the greatest improvement. This suggests that the main reason why No. 1 did not reach the calculated enhancement ratio was that the rigidity of the thin cylinder on the concave side was too high. No improvement in holding torque was observed for Nos. 4, 7, 9, and 11 with the groove element. Furthermore, there was an improvement for No. 5 with only the gear element, while the results for Nos. 8, 10, and 12 with the gear element and the slit or gap element were worse than those for No. 5. These results may be explained in that the thin cylinders are effortlessly deformed and the interlocking of the grooves fails when adopting the strategy of reducing the rigidity of the thin cylinder (with slit and gap elements).

4) Conclusion: We confirmed that increasing the number of friction surfaces improves the holding torque and found that the No. 6 unit performs best. To improve the holding torque, it is effective to reduce the rigidity of the thin cylinder by introducing slit and gap elements. As a result, the surface can make contact uniformly through deformation and increase the friction force. However, our discussion has not been able to deal quantitatively with changes in contact areas due to slit and gap. Quantitative evaluation of each element using computer simulation, e.g., finite-element method, is one of the future challenges. Furthermore, by modifying the gear, a large holding torque may be obtained by mechanical constraints (not friction). As another future challenge, we would like to use topology optimization to search for the geometry of thin cylinders where the wire tension (normal force) makes the gears meshed uniformly, and the external torque (shear force) makes it difficult for dislodged.

V. Vacuum Jamming Material

A. Consideration

We used a variable-stiffness pad fabricated using vacuum jamming materials to present stiffness/softness in the proposed device. The variable-stiffness pad requires a wide range of stiffness changes. Wall et al. [36] and Cheng et al. [37] verified that the use of coffee or paper realizes the most effective jamming. However, no study has examined or verified the material that maximizes the range of the stiffness change. We, therefore, examined the effect of inclusions and the bag thickness on

TABLE II
VACUUM JAMMING MATERIALS

No.	Inclusions	Thickness of bags
1	Coffee powder 2.5 g	1 mm
2	Coffee powder 1.8 g	1 mm
3	Paper stack 6 sheets and coffee powder 1.8 g	1 mm
4	Paper stack 30 sheets	1 mm
5	Paper stack 30 sheets	0.5 mm
6	Paper stack 30 sheets and sponge 4 mm	0.5 mm

the physical properties of vacuum jamming materials for the combinations of Nos. 1–6 in Table II.

The comparison of Nos. 1 and 2 verifies the effect of the amount of powder. The comparison of Nos. 2 and 3 reveals the interaction between powder and paper, and the comparison of Nos. 4 and 5 shows the effect of the bag flexibility. We compare Nos. 5 and 6 to confirm the characteristics of the sponge, which is normally highly flexible but loses its flexibility when compressed.

The paper (71 $\mathrm{g/m^2}$) and coffee powder that was extracted and dried were used as the inclusions. The inner dimensions of the bags were $100 \times 17.5 \times 3.2$ mm except in the case of No. 6, where the inner dimensions were set at $100 \times 17.5 \times 6.5$ mm to allow for the thickness of the sponge (4 mm). The bags were molded using silicon rubber.

B. Model of the Pushing Vacuum Jamming Material

Although the human sensory perception mechanism is complex, we defined a stiff/soft sensation as the load–displacement relationship. When a finger presses on the variable-stiffness pad, the center of the pad deflects. Therefore, the load–displacement relationship can be expressed as the deflection stiffness. Since deflection stiffness depends on the contact area with the finger, its absolute value does not perfectly correspond to the actual stiff/soft sensation. In this article, the relative change of deflection stiffness is regarded as a discriminative index of the stiff/soft sensation. In the following, we describe the modeling of the deflection stiffness of a compliant body.

One model used for plastic deformable compliant bodies is the nonlinear Maxwell model. In the nonlinear Maxwell model, the relationship of the load f, displacement x_1 of the nonlinear spring element, and displacement x_2 of the damper element is expressed as

$$f = kx_1^n = b\dot{x}_2 \tag{3}$$

where k is the coefficient of the nonlinear spring element, b is the coefficient of the damper element, and n is a real number (> 1). Stanley et al. [17] showed that the experimental results for the deflection x and the load f of the granular jamming are well explained by (3) in the case that $n = 2$. Therefore, from (3), the relationship between the load and overall deflection $x = x_1 + x_2$ is obtained as

$$x = x_1 + x_2 = \frac{1}{\sqrt{k}}\sqrt{f} + \frac{1}{b}\int_0^t f\, dt\,. \tag{4}$$

Here, the quadratic spring coefficient k represents the stiffness and the damper coefficient b represents the degree of plastic deformation of the granular jamming. To examine whether the same model can explain vacuum jamming materials other than granular materials, we measured the load and displacement when vacuum jamming materials are pushed as described in the next section. We then evaluated the stiffness/softness from the values of k and b calculated from the measured load and displacement.

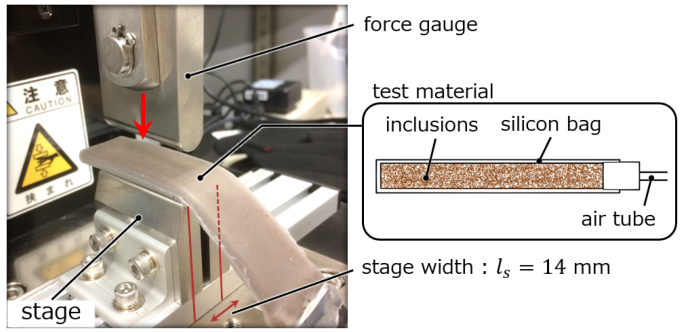

Fig. 6. Measurement of the quadratic spring stiffness and damping constant.

C. Comparison of Test Materials

1) Measurement Method: We performed a push-in test using the measurement device shown in Fig. 6. The spacing between the stages was set at 14 mm and the pushing distance was set at 3.5 mm with consideration of the width of the test materials. We carried out the following procedures ten times. 1) place the test material on the stage. 2) deflate the inside of the bag of the test material. 3) perform the push-in test and record the relationship between the applied force and displacement. The measurements were made under 18 conditions with three different vacuum patterns (vacuum pressure $p = 0, -20,$ and -40 kPa) for six materials.

2) Results: We consider the time series data of the force f_i and displacement x_i at the ith time step. Using (4), the measurement data can be expressed as

$$\boldsymbol{x} = F\boldsymbol{c} \tag{5}$$

where $F_i = \sum_{k=0}^{i} f_k \Delta t$ (Δt is the measurement interval) and

$$\boldsymbol{x} = \begin{pmatrix} \vdots \\ x_i \\ \vdots \end{pmatrix},\ F = \begin{pmatrix} \vdots & \vdots \\ \sqrt{f_i} & F_i \\ \vdots & \vdots \end{pmatrix},\ \boldsymbol{c} = \begin{pmatrix} \sqrt{1/k} \\ 1/b \end{pmatrix}.$$

Using the measurement data for each pressure p and each material, we obtained $k(p)$ and $b(p)$ for each material by finding the least-squares solution of $\boldsymbol{c}$ in (5). The results are shown in Fig. 7. Here, an error bar shows the standard deviation of measurements. Table III summarizes the characteristics of each material, such as the rate of stiffness change $\eta\ (= k_{\max}/k_{\min})$, the amount of change $\Delta k\ (= k_{\max} - k_{\min})$ against pressure, and the average $\overline{b}$ of the damper coefficient. In (4), η and Δk represent the range of the stiffness change of the variable stiffness pad, and the reciprocal of $\overline{b}$ represents the degree of plastic deformation.

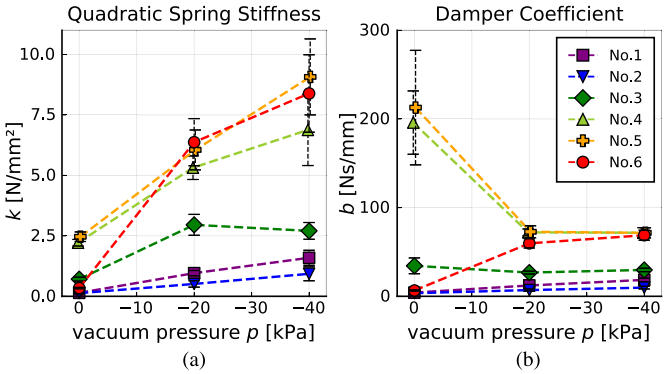

Fig. 7. Quadratic spring stiffness (k) and damping constant (b) at various pressures. Average values of ten measurements are plotted for each material and each pressure condition.

TABLE III
CHARACTERISTICS OF EACH TEST MATERIAL

No.	η	Δk [N/mm^2]	$\bar{b}$ [Ns/mm]
1	11.13	1.45	11.6
2	7.17	0.80	6.77
3	4.16	2.25	30.3
4	3.10	4.66	113
5	3.68	6.61	119
6	**24.63**	**8.05**	45.1

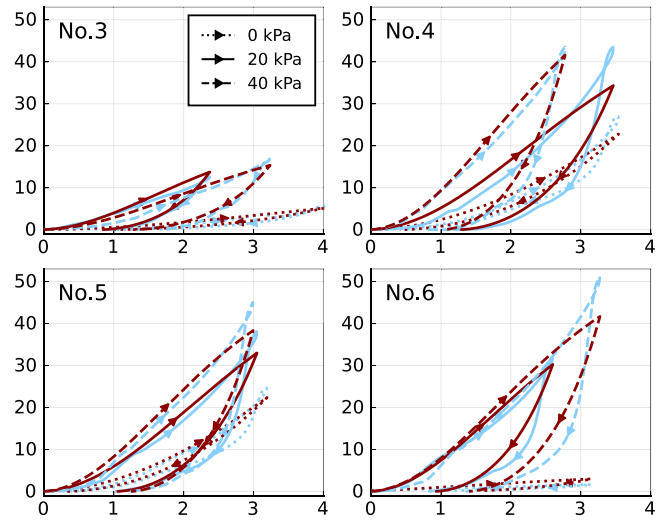

Fig. 8. Typical measurement force response (light blue) and theoretical force response (dark red).

Therefore, a material with large values of η, Δk, and $\bar{b}$ is evaluated as being suitable for developing the haptic device.

Fig. 8 shows a typical measurement curve (light blue) and a fitted model curve (dark red). The model curve was drawn by solving (4) numerically with a constant pressing speed $\dot{x} = 8.33$ mm/s, $k(p)$, $b(p)$ obtained from (5), and the initial value f_0 for each measurement.

We find that the model and the measurements are in good agreement in the region where the displacement is less than 3 mm from Fig. 8. We, therefore, conclude that model (4) proposed by Stanley adequately represents the characteristics of vacuum jamming materials other than granular materials.

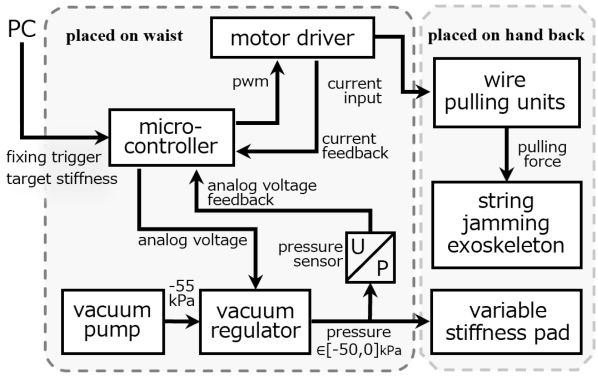

Fig. 9. Control system of the exoskeleton and variable-stiffness pad.

3) Discussion: According to Table III, we compare the six combinations in terms of the rate of change, amount of change, and damper coefficient. First, concerning the rate of change η, Nos. 1 and 2 with powder and No. 6 with the sponge layer have a larger rate of change than Nos. 4 and 5 with only the paper layer owing to their lower atmospheric stiffness ($k_{\min}$) at $p = 0$.

Table III shows that the change Δk is larger for Nos. 4–6 with the paper layer than for Nos. 1 and 2 without the paper layer. This is because the paper layer becomes stiff through compression in contrast with the coffee powder [36]. Additionally, comparing Nos. 1 and 2, we find that there is a larger stiffness change when there is more powder.

For No. 3 with both powder and paper layers, the adverse effects on both properties are particularly apparent, and both the rate η and amount of change Δk in stiffness were low. In contrast, for No. 6 with both sponge and paper layers, the positive effects of the sponge layer (which has high flexibility under atmospheric pressure) and the paper layer (which has high stiffness under vacuum) combine, and the rate η and amount of change Δk in stiffness are thus both large.

We finally compare the damper coefficient $\bar{b}$. The damper coefficient is smaller for Nos. 1 and 2 than for the other cases because no restorative force acts between the particles. In contrast, the damper coefficients of Nos. 3–6, which contain paper, are larger than those of Nos. 1 and 2. This is because the elasticity of the paper generates a restoring force after unloading.

The results for Nos. 4 and 5 reveal that the overall stiffness of the vacuum jamming materials is affected by the thickness of the silicon bag. In other words, using a thinner film, the stiffness of the inclusion itself can be presented without being affected by the softness of the silicon.

Considering the magnitudes of η, Δk, and $\bar{b}$, No. 6 having paper and sponge layers is considered effective in presenting softness/stiffness.

VI. PROTOTYPE DEVICE

We designed a prototype (Fig. 1) considering the experimental results in Sections IV and V. Fig. 9 is a block diagram of the control system, which was implemented on a microcontroller.

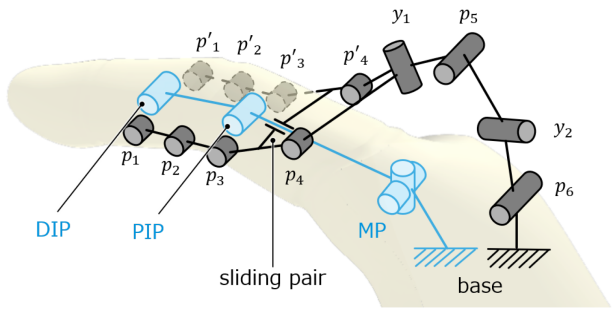

Fig. 10. Model of the proposed hand exoskeleton (gray) and common model of the finger kinematics (light blue). p_i indicates the front side of the paper and p'_i indicates the coaxial rotation axis at the back side.

Additionally, the prototype can be made completely wireless using wireless communications and a battery. The exoskeleton comprises rigid bodies, and it may, therefore, not be adjustable to the user's physique. However, the exoskeleton, which is made of resin parts constructed by a 3-D printer, can be easily reproduced in scaled forms. Furthermore, as described in Section VI-A1, the link mechanism of the exoskeleton has redundancy, such that there is no need to adjust it strictly to the user's body size. For these reasons, the exoskeleton can be easily adapted to different body sizes by preparing several sizes in advance.

A. Design of the Exoskeleton

This section describes the design of an exoskeleton mechanism that fixes finger movements and, thus, presents a braking force. Such a mechanism must satisfy two requirements. The first requirement is that the mechanism follow a finger's free movement. The second requirement is that the mechanism fix its shape during virtual grasping. A finger performs complex motions with a total of four DOFs, including two DOFs at the root joint (metacarpophalangeal (MP) joint) and two DOFs at the tip side (proximal interphalangeal (PIP) and distal interphalangeal (DIP) joints) shown in light blue in Fig. 10. Existing braking methods, such as the use of the magnetorheological brake [13], electrostatic brake [7] and layer jamming [14], do not brake motions of a finger.

In this article, we propose a link model that follows the arbitrary movements of the fingers in Section VI-A1. In Section VI-A2, we describe an exoskeleton that realizes the link model with the string jamming mechanism.

1) Link Mechanism Following Finger Motion: The movement of the exoskeleton should follow the rotation of the finger joints. The simplest method of realizing this function is to make the rotational axes coaxial with the finger joints. However, this method cannot tolerate a misalignment of the two axes [29], and a linkage mechanism with a redundant DoF [38] is, thus, adopted in this study.

First, we consider tracking the movement of the DIP and PIP joints on the tip side of a fingers. We arranged three rotational axes of the exoskeleton with one redundant DoF on the side of the finger, as shown in Fig. 10 (front side p_1-p_2-p_3; backside p'_1-p'_2-p'_3). In such an arrangement, the central rotation axis (p_2) affects the adjustment of the distance between the front and rear rotation axes (p_1, p_3). Therefore, the finger joints and rotation axes of the exoskeleton can be naturally aligned. For this reason, the links connecting p_1, p_2, and p_3 must be longer than the middle segment of the fingers (between DIP and PIP). In this study, the average length of each finger was calculated from hand dimension data [39], and one-third of the average length was used as the lengths of the links connecting p_1, p_2, and p_3.

Second, the MP joint has two DoFs (i.e., flexion/extension and adduction/abduction) and the rotational axes of the exoskeleton cannot be placed on the side of the finger because of interference with the back of the hand. We, therefore, adopted a different placement strategy. Here, we regarded the MP joint and the exoskeleton axes p_4, y_1, p_5, y_2, and p_6 as a "composite linkage," where the joint and axes are connected as follows. The link between p_6 and the base is completely fixed to the back of the hand and the link between p_3 and p_4 is constrained with one DoF to the finger root by the sliding pair. The exoskeleton rotational axes are then constructed so that the composite link has two DoFs, like the MP joint. By configuring the one-DoF rotational axes p_4, p_5, and p_6 parallel to the rotational axis of the finger flexion and then the one-DoF rotational axes y_1 and y_2 perpendicular to the axis in the order shown in Fig. 10, we configure the exoskeleton links such that there are DoFs of the composite link mechanism as for the MP joint. We calculate the number of DoFs of the composite link using the 3-D Kutzbach equation [40]:

$$\mathrm{DoF} = 6 \times (n_{\mathrm{link}} - 1) - (6-1) \times j_1 - (6-2) \times j_2 \quad (6)$$

where n_{link} is the number of links, j_1 is the number of one-DoF joints, and j_2 is the number of two-DoF joints. In this study, $n = 7$, $j_1 = 6$, and $j_2 = 1$ (for the MP joint). Therefore, there are two DoFs for the composite link. The total length of the links connecting p_4, y_1, p_5, y_2, and p_6 was determined so that no rotational axis would interfere with the MP joints. The size of the MP joint was set as the thickness of the hand (see [39]). The length of each link was determined by trial and error so that the radius of curvature of the inner wires was as large as possible.

As described above, we designed an exoskeleton with eight rotational axes that can follow the four-DoF movement of the finger as shown in Fig. 10 (gray).

2) Exoskeleton With a Shape Fixing Function: We realized the exoskeleton model devised in Section VI-A1 using string jamming to design a deformable and fixable exoskeleton glove (Fig. 11).

The developed exoskeleton has nine parts for each finger and eight-rotation axes connecting each part. Each part has thin cylindrical plates with the shape of a radial-layer jamming unit on each axis of rotation. Fig. 12 shows the basic shape. The layer number of thin cylinders was set at two according to strength and size limitations, and each joint thus has five friction surfaces ($N_{\mathrm{surfaces}} = 1 + 2N_{\mathrm{layers}}$).

Furthermore, on the basis of the results presented in Section IV, we applied slit and gap elements to each part so as to strengthen the holding torque. Fig. 12 shows an example of the improved parts. As shown in Figs. 11 and 12, two wires are threaded through the center of the rotation axis of each part. The two wires are connected to the pulley of the wire pulling unit

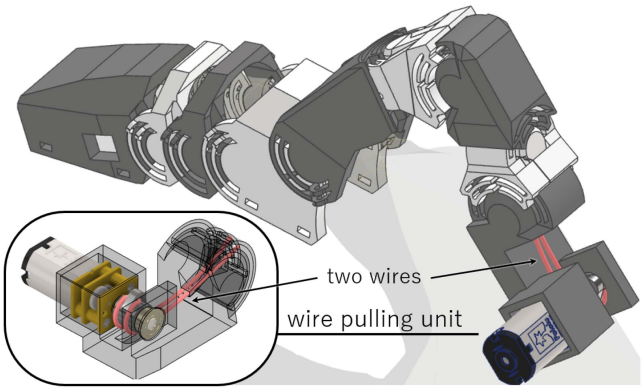

Fig. 11. Computer-aided design model of the proposed device (for one finger). The model comprises nine resin components made using a 3-D printer. The base component attached to the back of the hand is integrated with the wire pulling unit. Wires run through each component on either side of the finger, and the shape of the exoskeleton can be fixed by pulling the wires.

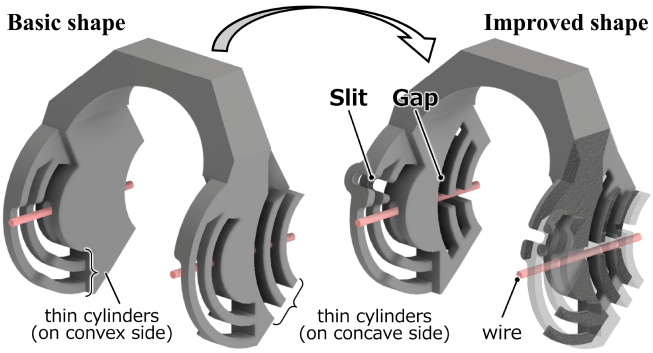

Fig. 12. Example of the basic shape (left) and improved unit (right) for the third unit from the tip of Fig. 11. The improved unit has slit and gap elements. Wires run on both sides of the inside of the parts, and through the pulling of the wires, a thin layer deforms and makes contact with the layer of the other unit.

that is integrated with the base unit fixed on the back of the hand as shown in Fig. 11. The wire pulling unit comprises a small motor (Pololu 1000:1 Micro Metal Gearmotor HPCB 12 V), a bearing, and a pulley and can pull the wire with a force of up to 120 N.

B. Design of the Variable-Stiffness Pad

We developed a variable-stiffness pad on the basis of the results in Section V. A bag was made from silicone (ecoflex 00-30), and a 4-mm sponge and 30 layers of paper ($71\mathrm{g/m^2}$) were included inside the bag. We determined the width of the sponge layer from the finger width (about 20 mm for the index finger, see [39]). The maximum stiffness reproduced by the variable-stiffness pad is determined by the center deflection of the pad, which depends on the width of the paper layer. A narrower paper layer results in higher maximum stiffness, but the width must be greater than the finger width to connect to the exoskeleton (see Fig. 13). The width of the paper layer was thus determined by trial and error so that it had the smallest width while connecting to the exoskeleton. As a result, the dimensions of the silicon bag were $80 \times 28 \times 8$ mm (1-mm thick) for the index finger.

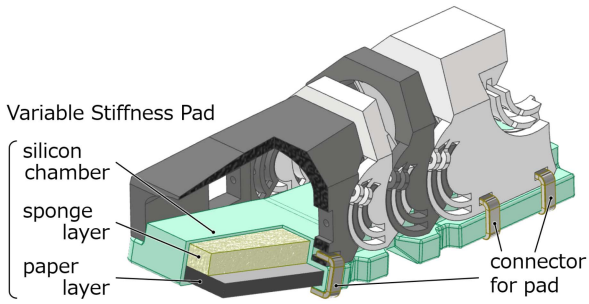

Fig. 13. Partial cross-sectional view of the variable-stiffness pad and connected exoskeleton.

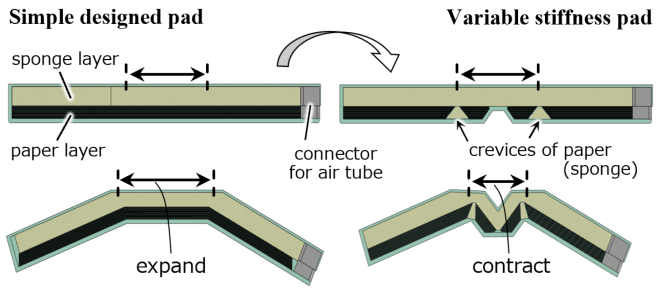

Fig. 14. Cross section of the variable-stiffness pad. Top left and right: Shape when a finger is extended for the simple designed pad and variable-stiffness pad. Bottom left: Shape of simple designed pad that disturbs the movement of a finger when it is bent. Bottom right: Shape of the variable-stiffness pad that does not disturb the movement of the finger when it is bent.

When a finger bends, the inner side of the finger contracts relative to the neutral configuration. Therefore, an ordinary jamming material with a simple pad design, as shown in Fig. 14 left, inhibits the bending motion of the finger. The variable-stiffness pad is structured to absorb the effect of the change in the finger belly length by dividing the inside paper layer into four sections, as shown in Fig. 14 right. In the left and right crevices, the paper layer was cut out and replaced with the sponges. In the middle crevice, the silicon bag's shape fits the crevice's shape to avoid the bag tearing when the pad is bent and the bag is stretched. The size of the crevices is about 8 mm at the center and 3 mm on the left and right. As the crevices are divisions along the long side of the paper layer and do not affect the width of the pad, the effect of the crevices on the stiffness presented by the variable-stiffness pad is limited.

We used three small diaphragm pumps (DSA-2F-24), an electronic vacuum regulator (ITV0091-2 L), and a pressure sensor (ZSE40AF-01-R-F) to control negative pressure in the variable-stiffness pad. The pressure can be controlled from 0 to -50 kPa in steps of 1 kPa. The pumps and regulator have a total weight of approximately 500 g, and they can be attached to the waist. Randazzo et al. [23] presented a comparison table of wearable devices and discussed portability for the weight of the main unit of each device. Compared with those weights, a weight of 500 g is sufficiently low.

VII. Performance Experiment

A. Analysis of the Actuation Speed

The shape fixing mechanism of the exoskeleton device is driven by pulling the wires. The time required for the transition from the relaxed state to the taut state of the wire was 0.32 s (average of 10 measurements and standard deviation of 0.034 s), corresponding to the 5% settling time of the step response of the motor current from 0 to 200 mA. To maximize the drive speed, proportional control was applied to the motor current and the feedback gain was tuned through trial and error. In the case of a device designed by Zubrycki et al. [14] using vacuum (layer) jamming to fix the finger shape, the 5% settling time was approximately 1.5 s (calculated from [14, Fig. 11]). The method of using vacuum jamming to brake increases the response time owing to the fluid friction and expansion of the air in the bag. In contrast, string jamming can respond more rapidly because the response time depends only on the electrical response time of the motor. Although the settling time of the developed device 0.32 ± 0.034 s is one-fifth that of Zubrycki et al.'s device [14], it is more than 0.2 s longer than the human tactile response [41], [42]. Further improvement is thus needed.

Next, for the variable-stiffness pad, to measure the response time of the stiffness change, we measured the 5% settling time for two responses: softening in which the internal pressure changes from -40 kPa to atmospheric pressure (0 kPa) and stiffening in which the internal pressure changes from atmospheric pressure to -40 kPa. The results show the settling time during the softening process was 0.25 ± 0.01 s. The softening process was not related to the number of pumps. In contrast, using three pumps in parallel, the stiffening process had a settling time of 0.73 ± 0.024 s. The curing time using one pump was 1.53 ± 0.031 s, and it is, thus, expected that the use of more pumps results in a faster transition to the vacuum in the stiffening process. However, three pumps considered the limit for a wearable device (where the combined mass of three pumps and one regulator is 500 g) owing to the device's weight.

Unlike the case of the presentation of the braking force, the variable-stiffness pad does not need to change stiffness at the same time as the virtual contact is made. It only needs to change in advance of the contact during the preshape movement of the user. Therefore, it is not a problem that the speed of the stiffness change is lower than the fixed speed of the exoskeleton.

B. Analysis of the Force Feedback

We measured the maximum value of the presentable braking force to verify whether the developed device can sufficiently present the sensation of the variable graspings. The experimental protocol was approved by the Ethics Committee, Graduate School of Engineering, Kyoto University (No. 202011).

An excessive holding torque of each joint deforms the exoskeleton because the string jamming mechanism is used to present the braking force. Therefore, the maximum braking force as a grasping sensation is equal to the maximum grip force of the user that does not deform the fixed exoskeleton.

In this study, we made measurements for the right index finger. As shown in Fig. 15(a), measurement points are the ventral surfaces of the terminal, middle, and basal segments and two points on each side of the finger. A thin-film force sensor (FSR-402) was applied at each of the seven points to measure the force felt by the finger.

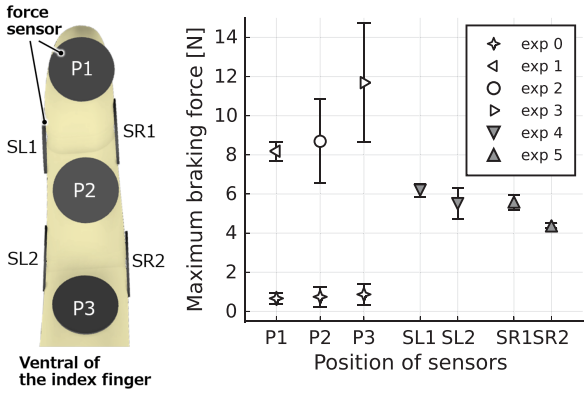

Fig. 15. Measurement of the maximum braking force and the resistance force for no braking. (a) Sensor positions. (b) Maximum force at each position.

First, we measured the maximum resistance force applied in the direction of flexion when the wire was not pulled and the device was free (exp 0).

Next, the wire was pulled at 120 N (corresponding to the maximum motor torque) and the device shape was fixed. A force was then applied gradually to the device by the user's finger, and the maximum force was recorded as the measurement at which the exoskeleton deformed. The user applied a force to the finger in the direction of flexion, and we measured the maximum force at the terminal segment P1 of the finger belly (exp 1), the maximum force at the middle segment P2 (exp 2), and the maximum force at the basal segment P3 (exp 3). To measure the maximum force at the lateral side of the finger, we also conducted experiments to measure the maximum force on the left side (SL1, SL2) by applying a force in the abduction direction (exp 4) and on the right side (SR1, SR2) by applying a force in the adduction direction (exp 5).

Fig. 15(b) presents the average of the 10 measurements. However, the variance in the measured values for P2 and P3 is substantial because it was difficult to apply a force to the same position.

Redmond et al. [43] found that the standard human grip force for daily grasping is about 7 N. The results of exp 1, 2, and 3 show that the developed device can present a maximum force of 8.0 N at the terminal part (fingertips), 8.5 N at the middle part, and 11 N at the basal part. Therefore, the prototype device achieves the standard of a person's daily grasping. In particular, the results of exp 2 and 3 show that the device can present a sufficient braking force on the middle and base of the finger. We find that the device can present a grasping force for the contact with the entire finger, unlike the case for existing devices, which only exert a localized force on the fingertip [8]–[13].

In addition, to our knowledge, there has been no analysis of the force applied to the finger side in human grasping. However, grasping using the lateral aspects of the fingers is generally performed when holding light objects such as keys or cigarettes.

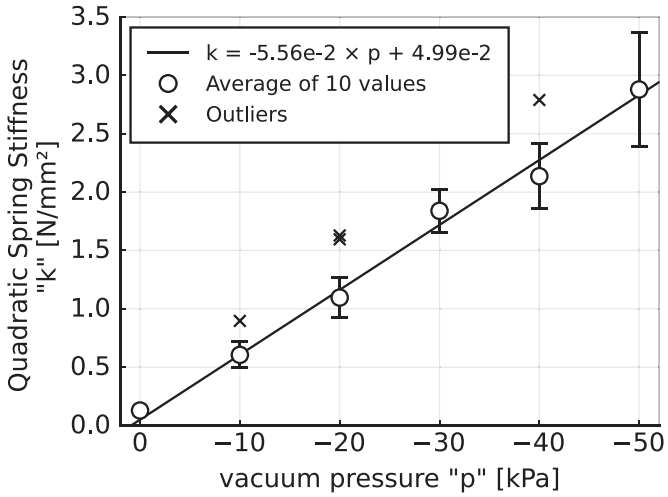

Fig. 16. Quadratic spring stiffness versus pressure in a variable-stiffness pad.

Therefore, the force applied in the adduction/abduction direction would be weaker than that applied in the flexion/extension direction. The results of exp 4 and 5 show that a braking force of approximately 6 N is applied on the abduction side (SL1 and SL2) and a braking force of approximately 6–4 N is applied on the adduction side (SR1 and SR2). While conventional devices only present a bending force [7]–[9], [12], [13], the proposed device presents the grasping sensation using the lateral sides of the fingers.

In our device design, we adopted the method of covering the entire finger like a glove and fixing the exoskeleton shape, such that the device presents passive feedback to a wide range of the finger (i.e., the lateral and ventral surfaces). This characteristic, which is not found for other devices, allows the presentation of force distributions that match the user's finger movements after preshaping. In other words, it is implicated that our device can present force distributions close to the grasping sensation expected by the user without controlling strictly.

Even when a user unconsciously intends to sense a force only on the fingertips, the middle and basal segments of the fingers are in contact with the device and the user feels a reaction force, although it is weak. This means that the user feels the reaction force in unexpected places when pinching a small virtual object. This issue can cause discomfort for the user. We may solve this problem by further developing a pad that can control the shape of the different surfaces of each segment independently in future work.

C. Resolution and Stiffness Range of a Variable-Stiffness Pad

We analyzed the presentable softness range and resolution of the softness of the variable-stiffness pad. The same experiment as described in Section V was carried out for the variable-stiffness pad. Measurements show that the damper coefficient was roughly constant at about 15 Ns/mm, and the relationship between the stiffness and internal pressure is shown in Fig. 16. Each data point is the average of 10 measurements and an error bar shows the standard deviation. A regression line is obtained using the least-squares method as

$$k(p) = -5.56\,e^{-2} \times p + 4.99\,e^{-2}\ (p \leq 0). \tag{7}$$

The system in Fig. 9 can control the internal pressure of the variable-stiffness pad from 0 to -50 kPa in steps of 1.0 kPa. The range of the variable stiffness is 56.9 times (= max/min), because the minimum stiffness is $4.99 \times 10^{-2}\mathrm{N/mm^2}$ ($p = 0\,\mathrm{kPa}$), and the maximum stiffness is $2.83\ \mathrm{N/mm^2}$ ($p = -50\,\mathrm{kPa}$). The resolution of the stiffness of the variable-stiffness pad is $5.56 \times 10^{-2}\mathrm{N/mm^2}$.

However, because the relationship between an actual physical property and human perception is rarely linear, it is essential to analyze the stiffness while focusing on the human subjective sensation. Studies on human stiffness perception have shown that the perception of object stiffness follows Weber's law; i.e., the minimum perceivable stimulus change is proportional to the stimulus intensity [44]–[46]. According to their research, the Weber fraction, a proportionality constant, is approximately 15% [44]. In other words, humans cannot perceive changes in stiffness within 15%.

Whereas other studies on stiffness perception [45], [46] focused only on the displacement/force ratio of the finger, Tiest et al. considered the effect of surface deformation in addition to the displacement/force ratio. They also reported that the Weber fraction is not affected by the thickness of the object or the separation of the fingers during the pinching motion [44]. The variable-stiffness pad of the proposed device deforms to present softness, and we should thus consider the deformation and conclude that the values of Tiest et al. are suitable for evaluation. Therefore, in presenting a continuous subjective stiffness change with the variable-stiffness pad, the condition is

$$\text{Weber fraction} = \left|\frac{\delta k}{k(p)}\right| = \frac{0.0556 \times \delta p}{k(p)} < 0.15. \tag{8}$$

When the pressure resolution $\delta p = 1$ kPa and $k(p)$ can be expressed by (7), the pressure region satisfying (8) is $p < -5.77$ kPa. Therefore, in this region, humans perceive a continuous stiffness change because the device can control the stiffness with preciseness better than human perception. Meanwhile, in the region of $-5.77 \leq p < 0$, the subjective stiffness changes discontinuously with a discretized change of 1 kPa, and there is an unpresentable softness. This aspect needs to be improved so that the pressure can be controlled more precisely.

The current variable-stiffness pad is a one-DoF system that regulates the vacuum pressure inside the cell, such that the stiffness and the damper coefficient cannot be controlled independently. However, it may be possible to create a flexible pad with an independently controllable stiffness and damper coefficient by dividing the cell into multiple layers of paper and sponge. In addition, we have not been able to analyze the correspondence between the perceived soft/stiff sensation in the real world and the absolute values of measured stiffness and damper coefficient. To intentionally reproduce specific flexible objects in VR, a greater understanding of soft/stiff perception is needed.

VIII. Conclusion

In this article, the goal is to present the sensations of different grasping of a compliant virtual object adapting to a user's motion (e.g., power/precision/intermediate grasping). We, therefore, developed an exoskeleton that fixes the finger motions and presents a braking force, and a flexible pad (variable-stiffness pad) that continuously changes in stiffness. Unlike existing methods, our exoskeleton has two features; i.e., it constrains the DoFs of the finger extension/flexion and abduction/adduction with only one actuator and it presents a braking force to the ventral and lateral surfaces of the fingers. Furthermore, because the variable-stiffness pad separates the heavy pump from the device itself, the device can be made lighter and smaller.

To overcome technical challenges in developing the exoskeleton, we developed a new string jamming unit shape that enhances the holding torque while keeping the interaxial distance short. The experimental results presented in Section IV show that effective strategies of enhancing the holding torque of the string jamming are to increase the number of friction surfaces and reduce the rigidity of the thin cylinders so that the surfaces can make contact with each other much more easily. As a result, we increased the holding torque by a factor of about 3 relative to the existing bead-type unit.

We examined the bag and inclusions of the vacuum jamming material, which greatly affect the stiffness, to increase the presentable stiffness range of the variable-stiffness pad. As shown in Section V, adding a sponge layer in addition to the paper layer used in the existing layer jamming technique was effective, and reducing the thickness of the outer membrane increases the maximum stiffness.

On the above basis, we developed a prototype and conducted evaluation experiments as reported in Section VII. We found that the maximum presentable force was 8.0 N at the fingertip, 8.5 N at the middle of the finger, and 11 N at the base of the finger. In other words, it was possible to present a braking force distribution below these values for each part. It was also found that a maximum braking force of 4–6 N could be presented to the side of the finger. In summary, we found that it is possible to present sensations such as those of power grasping and lateral grasping, which have been impossible to present with conventional devices [7]–[14]. Furthermore, the measurement of the reaction force of the variable-stiffness pad and the analysis of the Maxwell model revealed that the proposed device can present an object with a quadratic spring constant of 0.0499–2.83 $\mathrm{N/mm^2}$ and an almost constant damper coefficient. The Maxwell model can model many biological flexible tissues with hysteresis [17], and the presentation of stiffness by the variable-stiffness pads may therefore be used for human interaction.

As mentioned in Section VII, future work will involve improving the driving speed for fixing the exoskeleton shape and improving the spatial resolution of the presentable force. In particular, improving the fixation speed is important for immersion in the VR space. The speed could be improved using an electroactive polymer for wire tension instead of the present direct-current motor. Additionally, it is important to integrate with position sensors that acquire the hand back position (e.g., using a motion capture system) and the detailed shape of the fingers (e.g., using a data glove) to use this device as a haptic interface for VR. This integration is a task for future work. It is also necessary to increase the diversity of the characteristics of virtual objects that the variable-stiffness pad can reproduce. In particular, the quadratic spring coefficient and the damper coefficient cannot be controlled independently at present because of the single-DoF system, but it may be possible to solve this problem using a two-layer bag structure and controlling the vacuum pressure of each layer. Another challenge is to reproduce properties other than stiffness/softness simultaneously. If the temperature and texture of an object can be presented by a single pad (i.e., no longer a variable-stiffness pad), the number of applications as a haptic device will increase.

Acknowledgment

The authors would like to gratefully acknowledge Kenjiro Tadakuma and Rio Mukaide (Tohoku University) for their helpful expertise and invaluable discussions.

References

[1] N. Kamakura, M. Matsuo, H. Ishii, F. Mitsuboshi, and Y. Miura, "Patterns of static prehension in normal hands," *Amer. J. Occup. Ther.*, vol. 34, no. 7, pp. 437–445, 1980.

[2] M. R. Cutkosky, "On grasp choice, grasp models, and the design of hands for manufacturing tasks," *IEEE Trans. Robot. Autom.*, vol. 5, no. 3, pp. 269–279, Jun. 1989.

[3] F. Gonzalez, F. Gosselin, and W. Bachta, "Analysis of hand contact areas and interaction capabilities during manipulation and exploration," *IEEE Trans. Haptic*, vol. 7, no. 4, pp. 415–429, Oct./Dec. 2014.

[4] T. Feix, J. Romero, H. B. Schmiedmayer, A. M. Dollar, and D. Kragic, "The GRASP taxonomy of human grasp types," *IEEE Trans. Hum.–Mach. Syst.*, vol. 46, no. 1, pp. 66–77, Feb. 2016.

[5] C. L. Fernando et al., "Design of TELESAR v for transferring bodily consciousness in telexistence," in *Proc. IEEE Int. Conf. Intell. Robots Syst.*, 2012, pp. 5112–5118.

[6] G. Niemeyer, C. Preusche, and G. Hirzinger, "Telerobotics," in *Springer Handbook of Robotics*. Berlin, Heidelberg, Germany: Springer-Verlag, 2008, pp. 741–757.

[7] R. Hinchet, V. Vechev, H. Shea, and O. Hilliges, "Dextres: Wearable haptic feedback for grasping in VR via a thin form-factor electrostatic brake," in *Proc. 31st Annu. ACM Symp. User Interface Softw. Technol.*, 2018, pp. 901–912.

[8] CyberGlove Systems, "CyberGlove III–CyberGlove systems LLC." Accessed: Oct. 4, 2020. [Online]. Available: http://www.cyberglovesystems.com/cybergrasp http://www.cyberglovesystems.com/cyberglove-iii/

[9] M. Bouzit, G. Burdea, G. Popescu, and R. Boian, "The rutgers master II–New design force-feedback glove," *IEEE/ASME Trans. Mechatronics*, vol. 7, no. 2, pp. 256–263, Jun. 2002.

[10] T. Endo et al., "Five-fingered haptic interface robot: HIRO III," *IEEE Trans. Haptics*, vol. 4, no. 1, pp. 14–27, Jan./Mar. 2011.

[11] HaptxInc, "HaptX| Haptic gloves for VR training, simulation, and design." Accessed: Oct. 4, 2020. [Online]. Available: https://haptx.com/

[12] I. Choi, E. W. Hawkes, D. L. Christensen, C. J. Ploch, and S. Follmer, "Wolverine: A wearable haptic interface for grasping in virtual reality," in *Proc. 2016 IEEE/RSJ Int. Conf. Intell. Robot. Syst*., 2016, pp. 986–993.

[13] J. Blake and H. B. Gurocak, "Haptic glove with MR brakes for virtual reality," *IEEE/ASME Trans. Mechatronics*, vol. 14, no. 5, pp. 606–615, Oct. 2009.

[14] I. Zubrycki and G. Granosik, "Novel haptic device using jamming principle for providing kinaesthetic feedback in glove-based control interface," *J. Intell. Robot Syst.*, vol. 85, no. 3–4, pp. 413–429, 2017.

[15] T. Mitsuda, S. Kuge, M. Wakabayashi, and S. Kawamura, "Haptic displays implemented by controllable passive elements," in *Proc. IEEE Int. Conf. Robot. Automat.*, 2002, vol. 4, pp. 4223–4228.

[16] R. Mukaide et al., "Radial-layer jamming mechanism for string configuration," *IEEE Robot. Autom. Lett.*, vol. 5, no. 4, pp. 5221–5228, Oct. 2020.

[17] A. A. Stanley and A. M. Okamura, "Controllable surface haptics via particle jamming and pneumatics," *IEEE Trans. Haptics*, vol. 8, no. 1, pp. 20–30, Jan./Mar. 2015.

[18] R. L. Williams et al., "The virtual haptic back for palpatory training," in *Proc. 6th Int. Conf. Multimodal interfaces*, 2005, pp. 191–197.

[19] S. M. Feeman, L. B. Wright, and J. L. Salmon, "Exploration and evaluation of CAD modeling in virtual reality," *Comput.-Aided Des. Appl.*, vol. 15, no. 6, pp. 892–904, 2018.
[20] L. Dipietro, A. M. Sabatini, and P. Dario, "A survey of glove-based systems and their applications," *IEEE Trans. Systems, Man Cybern. Part C: Appl. Rev.*, vol. 38, no. 4, pp. 461–482, Jul. 2008.
[21] M. Fujiwara, K. Nakatsuma, M. Takahashi, and H. Shinoda, "Remote measurement of surface compliance distribution using ultrasound radiation pressure," in *Proc. IEEE World Haptics Conf.*, 2011, pp. 43–47.
[22] C. Pacchierotti, S. Sinclair, M. Solazzi, A. Frisoli, V. Hayward, and D. Prattichizzo, "Wearable haptic systems for the fingertip and the hand: Taxonomy, review, and perspectives," *IEEE Trans. Haptics*, vol. 10, no. 4, pp. 580–600, Oct./Dec. 2017.
[23] L. Randazzo, I. Iturrate, S. Perdikis, and J. D. Millán, "Mano: A wearable hand exoskeleton for activities of daily living and neurorehabilitation," *IEEE Robot. Automat. Lett.*, vol. 3, no. 1, pp. 500–507, Jan. 2018.
[24] F. Chinello, M. Malvezzi, D. Prattichizzo, and C. Pacchierotti, "A modular wearable finger interface for cutaneous and kinesthetic interaction: Control and evaluation," *IEEE Trans. Ind. Electron.*, vol. 67, no. 1, pp. 706–716, Jan. 2020.
[25] J. Iqbal, H. Khan, N. G. Tsagarakis, and D. G. Caldwell, "A novel exoskeleton robotic system for hand rehabilitation - conceptualization to prototyping," *Biocybernetics Biomed. Eng.*, vol. 34, no. 2, pp. 79–89, 2014. [Online]. Available: http://dx.doi.org/10.1016/j.bbe.2014.01.003
[26] D. Wang, M. Song, A. Naqash, Y. Zheng, W. Xu, and Y. Zhang, "Toward whole-hand kinesthetic feedback: A survey of force feedback gloves," *IEEE Trans. Haptics*, vol. 12, no. 2, pp. 189–204, Apr./Jun. 2018.
[27] X. Gu, Y. Zhang, W. Sun, Y. Bian, D. Zhou, and P. O. Kristensson, "Dexmo: An inexpensive and lightweight mechanical exoskeleton for motion capture and force feedback in VR," *Proc. CHI Conf. Hum. Factors Comput. Syst.*, 2016, pp. 1991–1995.
[28] I. M. Bullock, J. Borras, and A. M. Dollar, "Assessing assumptions in kinematic hand models: A review," in *Proc. IEEE RAS EMBS Int. Conf. Biomed. Robot. Biomechatronics*, 2012, pp. 139–146.
[29] M. Cempini, M. Cortese, and N. Vitiello, "A powered finger-thumb wearable hand exoskeleton with self-aligning joint axes," *IEEE/ASME Trans. Mechatronics*, vol. 20, no. 2, pp. 705–716, Apr. 2015.
[30] P. Ben-Tzvi and Z. Ma, "Sensing and force-feedback exoskeleton (SAFE) robotic glove," *IEEE Trans. Neural Syst. Rehabil. Eng.*, vol. 23, no. 6, pp. 992–1002, Nov. 2015.
[31] F. Kimura and A. Yamamoto, "A softness feeling display with an active tensioner controlling contact pressure distribution on a fingertip," *Appl. Mech. Mater.*, vol. 162, pp. 463–470, 2012.
[32] A. Bicchi, E. P. Scilingo, and D. De Rossi, "Haptic discrimination of softness in teleoperation: The role of the contact area spread rate," *IEEE Trans. Robot. Autom.*, vol. 16, no. 5, pp. 496–504, Oct. 2000.
[33] T. Endo, A. Kusakabe, Y. Kazama, and H. Kawasaki, "Haptic interface for displaying softness at multiple fingers: Combining a side-faced-type multifingered haptic interface robot and improved softness-display devices," *IEEE/ASME Trans. Mechatronics*, vol. 21, no. 5, pp. 2343–2351, Oct. 2016.
[34] M. Gentilucci, U. Castiello, M. L. Corradini, M. Scarpa, C. Umilta, and G. Rizzolatti, "Influence of different types of grasping on the transport component of prehension movements," *Neuropsychologia*, vol. 29, no. 5, pp. 361–378, 1991.
[35] N. Takemura, T. Fukui, and T. Inui, "A computational model for aperture control in reach-to-grasp movement based on predictive variability," *Front. Comput. Neurosci.*, vol. 9, pp. 1–15, Dec. 2015.
[36] V. Wall, R. Deimel, and O. Brock, "Selective stiffening of soft actuators based on jamming," in *Proc. IEEE Int. Conf. Robot. Autom.*, 2015, pp. 252–257.
[37] N. G. Cheng et al., "Design and analysis of a robust, low-cost, highly articulated manipulator enabled by jamming of granular media," in *Proc. IEEE Int. Conf. Robot. Autom.*, 2012, pp. 4328–4333.
[38] A. Schiele and F. C. Van Der Helm, "Kinematic design to improve ergonomics in human machine interaction," *IEEE Trans. Neural Syst. Rehabil. Eng.*, vol. 14, no. 4, pp. 456–469, Dec. 2006.
[39] M. Kouchi, "Japanese hand measurements." Accessed: Apr. 10, 2021. [Online]. Available: https://www.airc.aist.go.jp/dhrt/hand/index.html
[40] G. Gogu, "Mobility of mechanisms: A critical review," *Mechanism Mach. Theory*, vol. 40, no. 9, pp. 1068–1097, 2005.
[41] T. Miyasato, H. Noma, and F. Kishino, "Subjective evaluation of perception of delay time between visual information and tactile information," *J. Inst. Telev. Eng. Jpn.*, vol. 49, no. 10, pp. 1353–1356, 1995.
[42] S. Okamoto, M. Konyo, S. Saga, and S. Tadokoro, "Identification of cutaneous detection thresholds against time-delay and its effects on subjective feelings," in *Proc. 13th Robot. Symp.*, 2008, pp. 153–158.
[43] B. Redmond, R. Aina, T. Gorti, and B. Hannaford, "Haptic characteristics of some activities of daily living," in *Proc. IEEE Haptics Symp.*, 2010, pp. 71–76.
[44] W. M. Bergmann Tiest and A. M. Kappers, "Cues for haptic perception of compliance," *IEEE Trans. Haptics*, vol. 2, no. 4, pp. 189–199, Oct./Dec. 2009.
[45] H. Z. Tan, N. I. Durlach, G. L. Beauregard, and M.A. Srinivasan, "Manual discrimination of compliance using active pinch grasp: The roles of force and work cues," *Percept. Psychophys.*, vol. 57, no. 4, pp. 495–510, 1995.
[46] R. H. Lamotte, "Softness discrimination with a tool," *J. Neurophysiol.*, vol. 83, no. 4, pp. 1777–1786, 2000.

Ryohei Michikawa was born in 1997. He received the Diploma degree in mechanical engineering in 2020 from the Kyoto University, Kyoto, Japan, where he is currently working toward the Ph.D. degree in mechanical engineering with the Mechatronics Laboratory, Graduate School of Engineering.

His research interests include haptics and robotics.

Takahiro Endo (Member, IEEE) received the Dr.Eng. degree in computational intelligence and systems science from Tokyo Institute of Technology, Japan, in 2006.

He was an Assistant Professor with Gifu University, Gifu, Japan. Since 2015, he has been with the Department of Mechanical Engineering and Science, Kyoto University, Kyoto, Japan, where he is currently an Associate Professor. His research interests include haptics, robotics, and the control of infinite dimensional systems.

Fumitoshi Matsuno (Senior Member, IEEE) received the Dr.Eng. degree in control engineering from Osaka University, Toyonaka, Japan, in 1986.

In 1986, he joined the Department of Control Engineering, Osaka University. Since 2009, he has been a Professor with the Department of Mechanical Engineering and Science, Kyoto University, Kyoto, Japan. His research interests include robotics, swarm intelligence, control of nonlinear and distributed parameter systems, etc.

Dr. Matsuno was the recipient of awards, including the Best Paper Awards in 1986 from ISCIE, in 2001, 2006, and 2017 from the Society of Instrument and Control Engineers (SICE), in 2013 from the Information Processing Society of Japan, in 2018 from the RSJ, and the Prize for Academic Achievement from Japan Society of Mechanical Engineers (JSME) in 2009. He was a General Chair of *International Symposium of Distributed Autonomous Robotic Systems (DARS) 2021* and *Asian Control Conference (ASCC) 2022*. He also served as a General Chair of *IEEE SSRR2011*, *IEEE/SICE SII2011*, *SWARM2015*, *SWARM2017*, etc. He is a Fellow Member of SICE, JSME, and RSJ. He is the Vice-President of the NPO Int. Rescue System Institute and served as the President of the Institute of Systems, Control, and Information Engineers (ISCIE) and the Vice-President of the Robotics Society of Japan (RSJ).